

# Quantum Science and Technology



PAPER

OPEN ACCESS

RECEIVED  
4 March 2022REVISED  
28 July 2022ACCEPTED FOR PUBLICATION  
4 August 2022PUBLISHED  
25 August 2022

Original content from this work may be used under the terms of the [Creative Commons Attribution 4.0 licence](#).

Any further distribution of this work must maintain attribution to the author(s) and the title of the work, journal citation and DOI.



## GHz-pulsed source of entangled photons for reconfigurable quantum networks

Meritxell Cabrejo-Ponce<sup>1,2,\*</sup> , Christopher Spiess<sup>1,2</sup> , André Luiz Marques Muniz<sup>2</sup>, Philippe Ancsin<sup>2</sup> and Fabian Steinlechner<sup>2,3,\*</sup> 

<sup>1</sup> Friedrich Schiller University, Max-Wien-Platz 1, 07743 Jena, Germany

<sup>2</sup> Fraunhofer Institute for Applied Optics and Precision Engineering, Albert-Einstein-Str. 7, 07745 Jena, Germany

<sup>3</sup> Abbe Center of Photonics, Friedrich Schiller University Jena, Albert-Einstein-Str. 6, 07745 Jena, Germany

\* Authors to whom any correspondence should be addressed.

E-mail: [meritxell.cabrejo.ponce@iof.fraunhofer.de](mailto:meritxell.cabrejo.ponce@iof.fraunhofer.de) and [fabian.steinlechner@iof.fraunhofer.de](mailto:fabian.steinlechner@iof.fraunhofer.de)

**Keywords:** quantum communications, polarization entanglement, phase modulation, reconfigurable quantum networks, fiber-based

Supplementary material for this article is available [online](#)

### Abstract

Entanglement is a universal resource in quantum networks, yet entangled photon sources are typically custom-made for a specific use case. Versatility, both in terms of state modulation and tunability of the temporal properties of the photons, is the key to flexible network architectures and cryptographic primitives that go beyond quantum key distribution. Here, we report on a flexible source design that produces high-quality entanglement in continuous-wave and GHz-rate-pulsed operation modes. Utilizing off-the-shelf optical components, our approach uses a fiber-based Sagnac loop to generate polarization-entangled photons at telecom wavelength with high efficiency and fidelities above 0.99. Phase modulation up to GHz before entangled state generation is also possible for fast entangled state switching. We show phase modulation at 100 MHz with an average fidelity of 0.95. Furthermore, the source 60 nm spectral bandwidth is entirely compatible with fully reconfigurable wavelength-multiplexed quantum networks.

## 1. Introduction

Entangled photons are an essential resource in emerging quantum information processing and secure quantum communications [1, 2]. In the context of quantum cryptography, entanglement-based quantum key distribution has recently received considerable attention due to its inherent simplicity. It leverages the intrinsic randomness of quantum entanglement and can be implemented with passive optical components [3, 4]. Moreover, it allows for scalable multiuser operation through the use of auxiliary frequency correlations for multiplexing [5, 6]. However, richer cryptographic primitives and beyond require more flexibility from the source. For example, entanglement swapping and other protocols that rely on interference of independent sources usually require pulsed quantum sources [7], but are recently extending to continuous-wave (CW) regimes [8]. On the other hand, fast state control is also required for reconfigurable quantum networks [9] and particularly for protocols such as three-partite quantum secret sharing (QSS), that need phase modulated entangled states [10].

Typical sources are those of polarization entangled qubits, often consisting of free-space interferometers based on bulk optics [11]. They provide stable operation and high photon-pair rates by employing spontaneous parametric down-conversion (SPDC) processes in  $\chi^{(2)}$ -nonlinear crystals or waveguides. However, the dimensions of the bulky components make it difficult for the source to be reconfigurable and especially fast. They are optimized to be solely used for CW or in pulsed regimes and are not easily interchangeable. Furthermore, pump and down-converted photons frequently need to propagate along the same paths, involving the use of expensive dual-wavelength components to achieve high visibility [12–14].

A lot of effort has been directed toward the realisation of polarization entangled photon sources (EPSs) with both pump and correlated photons in telecom wavelengths. In this manner, inexpensive high-speed

optical modulators and communication through the already existing global fiber network could be exploited. The natural choices for those systems are  $\chi^{(3)}$  materials via spontaneous four wave mixing, since they enable both pump and photon-pairs in the same wavelength bands [15, 16]. They can be integrated in polarization maintaining (PM) fiber Sagnac interferometers, which provide great phase stability [17, 18]. Nevertheless, their bulk nonlinearity is  $10^4$ – $10^5$  orders of magnitude smaller than cascaded  $\chi^{(2)}$  processes (i.e. second harmonic generation (SHG) and SPDC in the same  $\chi^{(2)}$  material) [19–22].

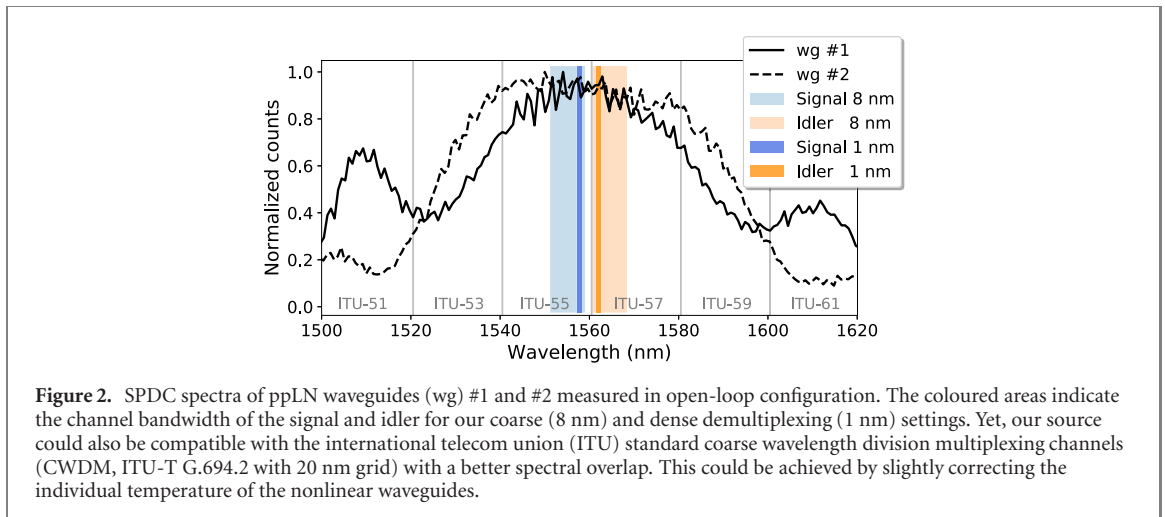
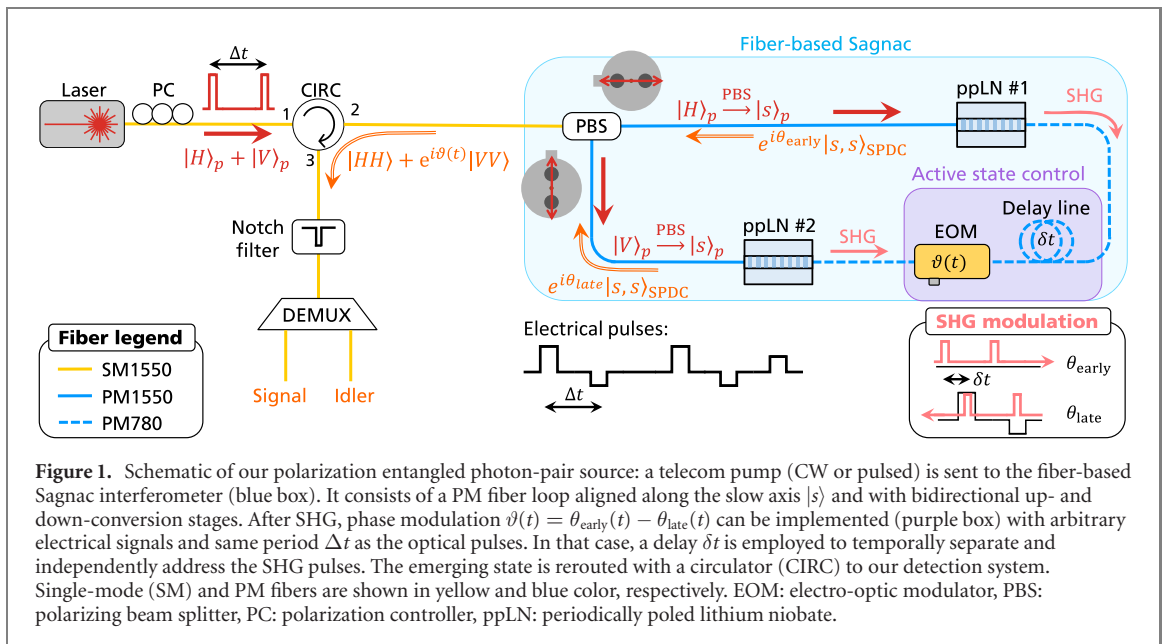
In this letter, inspired by the work in [23–25] for faint-pulse sources (i.e., a classical laser attenuated to the single photon level) and motivated by the efficient generation of photon-pairs in waveguides [26–28], we propose a novel EPS at telecom wavelengths based on a fiber-based Sagnac interferometer with two  $\chi^{(2)}$  nonlinear waveguides. In this configuration, a telecom pump enters the fiber loop and follows a cascaded up- and down-conversion process in both directions. The immediate advantage is that the source does not need dual-wavelength components like the free-space versions. Additionally, the design allows the incorporation of fiber-integrated optical modulators to (i) easily switch the pump from CW to GHz-pulsed regimes, and (ii) to modulate the phase of the generated state up to GHz rate. To demonstrate the versatility of this source, we characterize it in CW and GHz-pulsed regimes in terms of photon pair generation and visibility as a function of repetition rate and duty cycle for coarse and dense wavelength division multiplexing (WDM) arrangements. We report Bell-state fidelities above 0.99 for different pump configurations and high brightness, with millions of photons at emission per nm of bandwidth. The spectrum spans over 60 nm, offering the possibility to increase the number of users via wavelength demultiplexing or to actively allocate the necessary bandwidth in a practical scenario [29].

Finally, to showcase the ultimate flexibility of our design, we continuously switch the generated entangled state from a basis of four different states. In this proof-of-concept experiment, we achieve average state fidelities of 0.95 at 100 MHz rate. These results are a step forward towards a fully reconfigurable EPS and may pave the way for active quantum networks.

## 2. Entangled photon source

Our fiber-based Sagnac loop is pictured in figure 1. After pump preparation (see methods), the pump polarization is set with polarization controllers (PC) right before a polarization beam splitter (PBS). This is  $|\Psi_p\rangle = \frac{1}{\sqrt{2}}(|H\rangle_p + e^{i\phi_p}|V\rangle_p)$ , where  $\phi_p$  is a phase term that can be included in the final entangled state. For the sake of brevity, we omit this relative phase in the following discussion. The fiber PBS accordingly separates  $H$ - and  $V$ -components and sends them over polarization-maintaining (PM) fibers. Here, the transmission and reflection ports are aligned to the slow axis of the fibers, denoted as  $|s\rangle$ , meaning that one of the PM fibers is physically rotated by  $90^\circ$ . Thus, the incoming  $H$  and  $V$  polarizations of the pump beam travel along the same (slow) axis of the PM fiber inside the loop such that group velocity mismatch is compensated. The outputs of the PBS are connected to two fiber-pigtailed periodically poled lithium niobate (ppLN) waveguides (Covesion MSHG1550 with 40 mm long type-0 crystal). These are commercially available SHG modules, where a 1550 nm PM fiber is directly coupled to a ppLN waveguide and a 780 nm PM fiber is coupled at the other end. They have slightly different SHG conversion efficiencies due to fabrication imperfections, 10% and 11% respectively for 300 mW of pump power. Yet, this difference can be compensated with a small rotation of the pump polarization. The highest SHG conversion is achieved by tuning the temperature of the ppLN waveguides #1 and #2 ( $53^\circ\text{C}$  and  $48^\circ\text{C}$  respectively), which simultaneously produces broadband pair generation around a degeneracy wavelength of 1560 nm. The SPDC spectrum spans over the C-band and beyond (from 1530 to 1590nm) with the full width at half maximum of 58 nm and 68 nm for waveguide #1 and #2 respectively, as shown in figure 2. Finally, both ppLN modules are interconnected with a 780 nm PM fiber to close the loop. As a result, the second harmonic generated light of one waveguide is sent to the opposite one to generate SPDC and vice versa. This situation occurs in both clockwise and counterclockwise directions, whereby the physical rotation of the PM fiber at the PBS gives rise to a polarization-entangled state. For active state switching, as explained at the end of this letter, we can introduce here a delay line to temporally separate the SHG pulses that travel in opposite directions (see inset in figure 1), and an electro-optic modulator (EOM) to modulate their relative phase  $\vartheta(t)$  (purple box in figure 1).

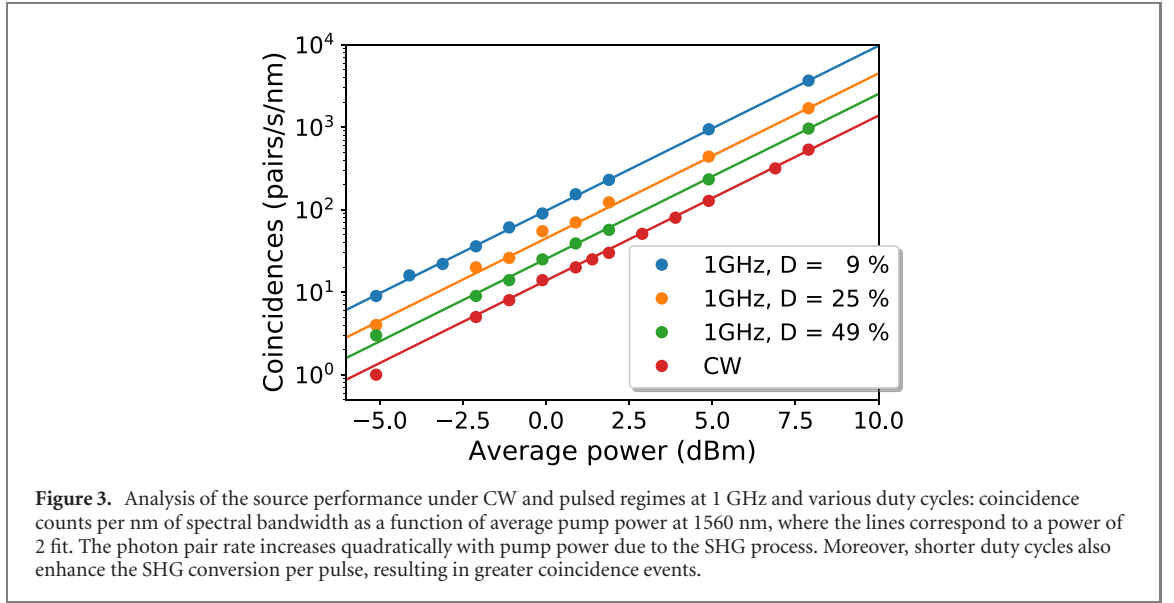
In this configuration, SPDC photon pairs emerge in the entangled state  $|\phi\rangle = \alpha|H_s H_i\rangle + e^{i\vartheta(t)}\beta|V_s V_i\rangle$ , where  $H_{s(i)}$  is the signal (idler) photon in the  $H$  polarization, and similarly for  $V$ . In the remaining, we suppress the subscripts of the state. Here,  $\alpha$  and  $\beta$  are the probabilities of generating SPDC photon-pairs clockwise and counterclockwise, respectively, while  $\vartheta(t)$  denotes the detuning phase between both directions. By optimizing the pump polarization and without SHG modulation,  $\alpha = \beta = 1/\sqrt{2}$  and  $\vartheta = 0$ , resulting in the maximally entangled Bell state  $|\phi^+\rangle$ . The outgoing light from the PBS is rerouted via the circulator (CIRC) followed by a 100 dB notch filter, with 1.6 nm bandwidth at 1560 nm, that removes any



remaining fraction of the pump or additional noise. Note that not much filtering should be needed considering that the 780 nm fiber in the loop largely suppresses the 1560 nm pump. Additionally, any perturbation on the fiber loop affects simultaneously both propagation directions, maximizing phase stability of the entangled state. Finally, the signal and idler correlated photons are separated by a demultiplexer (DEMUX) to be sent to independent users. Here, we directly send them to our detection system (see methods).

### 3. Performance analysis

We first characterize our source excluding the active state control elements. In our narrowband WDM scheme, the signal and idler channels selected by the programmable filter are separated by 3.2 nm with a bandwidth of  $\Delta\lambda = 1$  nm, as shown in figure 2. We report in figure 3 the photon-pair coincidence counts per nm of spectral bandwidth, a parameter known as the spectral brightness, as a function of the average pump power ( $P_{\text{in}}$ ) right before the PBS, for CW and pulsed operation at repetition rates of 1 GHz and duty cycles of 9%, 25% and 49%. These measurements are performed with  $H$  polarization settings for both the signal and the idler SPDC photons, which represent the performance of a single direction of the loop. The coincidence counts grow with a power of 2 and are proportional to  $P_{\text{in}}^2$  (fitted in figure 3), according to the quadratic SHG power conversion and the linear SPDC power conversion. Furthermore, shorter duty cycles yield stronger SHG at the same average but higher peak pump power, and therefore, higher SPDC brightness. The photon-pair heralding, defined as the ratio of coincidences over single-photon counts,



improves with pump power and shorter duty cycle because of a relative reduction of additional noise sources (see supplementary material (<https://stacks.iop.org/QST/7/045022/mmedia>)). It amounts to  $H_s = 1.6\%–2.9\%$  and  $H_i = 2.9\%–5.2\%$  for signal and idler, respectively, differences that can be explained by the accumulated and asymmetric losses in the system as well as the coupling efficiency of the ppLN waveguide modules. With a total loss of  $\sim 12.85$  dB (see methods), the actually emitted heralding is almost 20-fold higher.

To verify the quality of the entanglement, polarization projecting measurements are performed in two mutually unbiased bases,  $H/V$  and  $D/A$ , for different pump parameters. In the  $H/V$  basis and for the state  $|\phi^+\rangle$ , the visibility per nm of spectral bandwidth is computed as:

$$V_{HV} = \frac{R_{HH} - R_{VH} - R_{HV} + R_{VV}}{R_{HH} + R_{VH} + R_{HV} + R_{VV}} \quad (1)$$

where  $R_{ij}$  denotes the coincidence rate measured with  $i, j$  settings, and similarly for  $D/A$ . We find that for a 1 GHz repetition rate, 9% duty cycle and 7.9 dBm of pump power right before the PBS, we achieve visibilities of 99.5% in  $H/V$  and 99.0% in  $D/A$ , with no subtraction of accidentals. Using the fidelity witness  $F \geq (V_{HV} + V_{DA})/2$  [11], we lower-bound the Bell-state fidelity to  $F = 99.25\%$ .

We also quantify the quality of entanglement for a coarse WDM scheme. The broadest filter we can set for our source with our programmable filter is 8 nm bandwidth, although broader channels should also be possible with different DEMUX. We use this setting for both the signal and idler, separated by a notch of 1.6 nm (as shown in the light gray area in figure 2). The pump power is set to 9.0 dBm just before the PBS at an 8 GHz pulsed regime and 50% duty cycle, the fastest pump rate we can set with our current electrical devices. We observe visibilities of  $V_{HV} = 99.4\%$  and  $V_{DA} = 97.7\%$ , with no subtraction of accidentals. The lower bounded fidelity is thus  $F \geq 98.6\%$ .

The detected pair rate at 12.85 dB loss is  $R_{HH} = 8027$  and  $R_{VV} = 7812$ , with a heralding of 1.7% for the signal and 3.4% for the idler photon with respect to the averaged  $|HH\rangle$  and  $|VV\rangle$  projection settings. The actual emission rates can be estimated by compensating for the loss such that  $R^{\text{est}} = R^{\text{exp}}/\eta_s\eta_i$ , with  $R^{\text{exp}}$  the experimental measurement,  $\eta_s = 6.6\%$ ,  $\eta_i = 4.1\%$  (see methods), and amounts to 5.9 Mpairs/s at this power and channel bandwidth. By replacing several parts of our detection system with commercially available low-loss components, the losses could be reduced at least by 10 dB. In that case, the usable photon pairs would be in the order of 1.6 Mpairs/s with a heralding of 20%–30%. Such high photon rates would already saturate many of the current commercial single photon detectors and time tagging systems and therefore, one would usually need to work with lower power values. We note, however, that state-of-the-art SNSPD array detectors can reach up to GHz detections [30]. Furthermore, the average emitted photon rate in all these measurements is  $\sim 0.001$  per pulse, such that multi-pair emission can be neglected [31]. We remark that this value of the mean photon pair rate per pulse can be increased with higher pump power, but it is chosen to be low here to avoid saturation of the detectors.

The emitted brightness with respect to the 1560 nm pump is 93.3 kpairs/s/mW<sup>2</sup>. However, to compare our system with other  $\chi^{(2)}$  sources, the estimated power of the second harmonic at 780 nm can be used for

**Table 1.** Detected and estimated photon pair rates ( $R^{\text{exp}}$  and  $R^{\text{est}}$ ) and heralding values for signal and idler photons ( $H_s^{\text{exp}}$ ,  $H_i^{\text{exp}}$  and  $H_s^{\text{est}}$ ,  $H_i^{\text{est}}$ ) at the output of the EPS (i.e. after the PBS) for one polarization projection  $|\Psi_{\text{proj}}\rangle = |HH\rangle$ . Notice that the heralding is limited by the coupling of the fibers to the ppLN waveguides.  $P_{\text{in}}$ : input pump power right before the PBS,  $\Delta\lambda$ : signal and idler channel bandwidth.

Pump rep. rate	Duty cycle (%)	$P_{\text{in}}$ (dBm)	$\Delta\lambda$ (nm)	$R^{\text{exp}}$ (pairs/s)	$H_s^{\text{exp}}$ (%)	$H_i^{\text{exp}}$ (%)	$R^{\text{est}}$ (Mpairs/s)	$H_s^{\text{est}}$ (%)	$H_i^{\text{est}}$ (%)
CW	100	7.9	1	535	1.6	2.9	0.20	39.8	44.2
1 GHz	9	7.9	1	3672	2.9	5.2	1.36	71.6	79.0
	49	7.9	1	963	2.1	3.8	0.36	51.4	57.6
4 GHz	44	7.9	1	901	2.1	3.8	0.33	51.7	57.3
8 GHz	50	7.9	1	565	1.9	3.3	0.21	45.5	50.0
	50	9.0	8	8027	1.7	3.6	2.98	41.6	54.0

normalization, which is  $3 \mu\text{W}$  per SHG module at this pump power. In this case, the emitted total pair rate corresponds to 1 Gpair/s/mW. To conclude, we summarize the results of this section in table 1.

This characterization (extended in the supplementary) shows that brightness and heralding in our source improve with shorter duty cycle and that our design can be used for any repetition rate (as long as fiber dispersion does not affect). In our experiment, the highest repetition rate (8 GHz) and shortest pulse width ( $\sim 70$  ps) are driven at the limit of our electrical pulse generator. Thus, deteriorated electrical signals eventually deform the optical pulse, leading to lower spectral brightness. Yet, our design is not only restricted to pulsed operation, since good figures of merit are also obtained for CW pump. In that case, cheap laser diodes could be employed instead of our involved pulse preparation scheme (see methods). Additionally, since our source spans over 60 nm of bandwidth, multiple demultiplexed channels can be used with large photon numbers and potentially high interference visibility. We note that a better spectral overlap between both ppLN modules would be needed to achieve high visibility.

#### 4. Active state control

Finally, we investigate the fast switching capabilities of the polarization-entangled state phase as a basic prerequisite for active quantum networks. Since the final state depends on the relative phase between the SHG pulses, it is enough to modify the phase of only one of them (lower right inset in figure 1). For this purpose, a phase modulator and a PM fiber delay line of 1 m length are inserted between the ppLN waveguides, as shown in figure 1. In this manner, the SHG pulses that travel along the counter-clockwise direction traverse the EOM first, which introduces a phase  $\theta_{\text{early}}$ , followed by the delay line. The pulses traveling in the clockwise direction encounter an additional delay before they acquire the phase  $\theta_{\text{late}}$  from the EOM. Since the length of the interferometer is the same in both directions, the SPDC probability amplitudes of both paths are perfectly recombined at the output even after SHG modulation.

When no voltage is supplied to the EOM, and if a diagonal pump polarization is fed into the loop as described previously, the state remains the same:

$$|\phi^+\rangle = \frac{1}{\sqrt{2}}(|HH\rangle + |VV\rangle) \quad (2)$$

However, if  $V_\pi$  is applied to one of the pulses, i.e.  $\vartheta = \theta_{\text{early}} - \theta_{\text{late}} = \pi$ , then the entangled state becomes:

$$|\phi^-\rangle = \frac{1}{\sqrt{2}}(|HH\rangle - |VV\rangle) \quad (3)$$

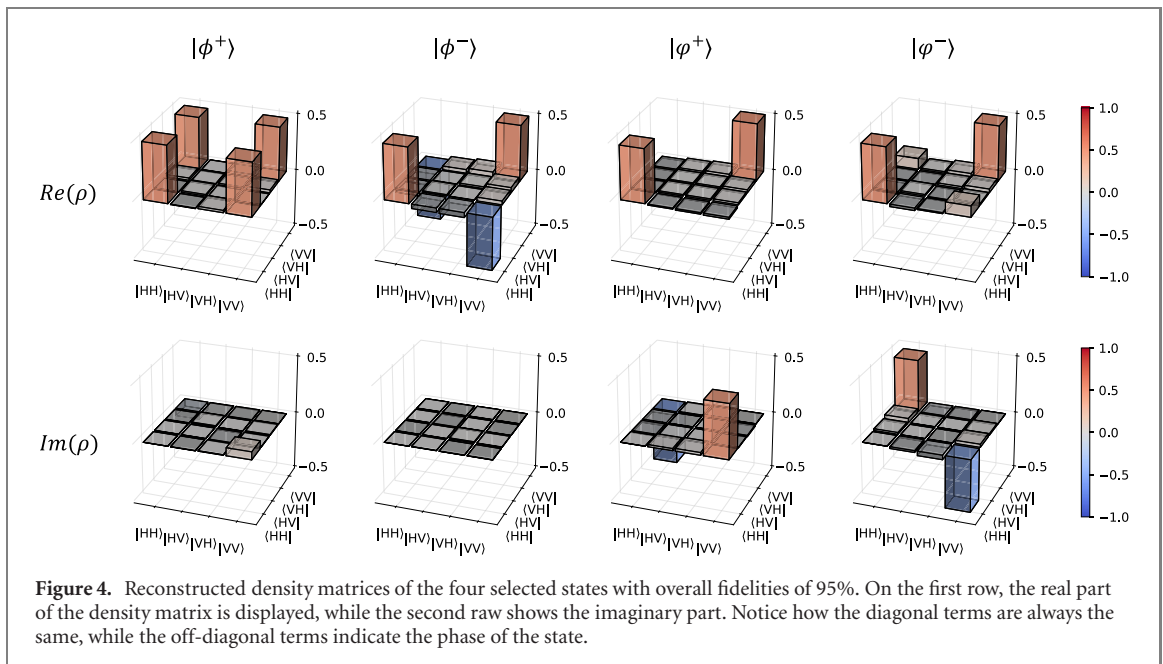
which is another maximally entangled Bell state. Nonetheless, we can also generate other states that are necessary for cryptographic primitives such as QSS [9]. We choose the ‘ $i + /i-$ ’ states:

$$|\varphi^+\rangle = \frac{1}{\sqrt{2}}(|HH\rangle + i|VV\rangle) \quad (4)$$

$$|\varphi^-\rangle = \frac{1}{\sqrt{2}}(|HH\rangle - i|VV\rangle) \quad (5)$$

that just require  $\pm V_{\pi/2}$  voltage for the EOM. If the phase is introduced to the first pulse, the sign of the voltage transfers to the phase in the superposition. If introduced to the second pulse, then the sign of the phase is inverted. One can also restrict only to positive voltages by applying  $+V_{\pi/2}$  either to the first or the second SHG pulse to alternate between these two states.





We perform the phase modulation experiment by using the second channel of our electrical signal generator, which allows us to fine-tune the time and amplitude of the RF electrical pulses that feed the EOM. These pulses are generated at a 100 MHz rate and have a duty cycle of 5%. The pulse amplitude is chosen from the voltage set  $\{0, +V_{\pi}, -V_{\pi/2}, +V_{\pi/2}\}$ , targeting the second and delayed SHG pulse (see methods). The optical pulses are generated at the same repetition rate and duty cycle of 1%, with an average power of 5 dBm before the PBS. Note that the losses of the EOM account for 3.5 dB, but only affect the SHG stage and do not deteriorate the final entangled state. The filter settings are again 8 nm bandwidth for the signal and idler channels, as in figure 2, and their polarization state is analyzed in our detection system (see methods). The measured coincidence rate reaches 4.5 kpairs/s per polarization setting, again after  $\sim 12.85$  dB loss in our setup. We measure the full-state tomography to reconstruct the density matrix and apply maximum likelihood estimation to obtain a physical one [32, 33]. The final results are presented in figure 4.

With little optimization effort, we achieve fidelities of 95.0%, 95.0%, 95, 8% and 94.3% for the states  $|\phi^+\rangle$ ,  $|\phi^-\rangle$ ,  $|\varphi^+\rangle$  and  $|\varphi^-\rangle$  respectively. These measurements are performed in one run by integrating over 100 ms per polarization setting and averaging over ten samples, while the same periodic RF electrical pulse is employed continuously to modulate the state phase. To change the state, we only change the pulse sequence at the electrical pulse generator. Nevertheless, our signal generator and common RF sources can also be fed with a very long sequence of arbitrary pulses among the set of four. In that case, a state switching at a 100 MHz repetition rate would occur. Even higher switching rates up to GHz are possible, but are eventually limited to the propagation time of the pulses in the phase modulator.

## 5. Conclusion

We have developed and experimentally evaluated a fiber-based Sagnac interferometer that utilizes standard telecom components to generate high-quality polarization-entangled states for a variety of pulse rates and duty cycles. We show that our source can be easily employed in CW up to GHz-pulsed regimes, with the latter being more suitable due to the stronger SHG and SpRS noise reduction and hence higher brightness and CAR. We obtain fidelities of 0.99 and generate millions of photon pairs per nm of spectral bandwidth, while the source spectrum extends 60 nm. Although our detection rates are considerably affected by the loss in the optical components used to characterize the source, most notably the DEMUX, these numbers would be substantially improved using commercially available low-loss components. We also prove great entanglement quality after active state switching at 100 MHz rates with fidelities up to 0.95. While not experimentally demonstrated here, we note that the source scheme is also ideally suited to the generation of hyperentanglement in the time-energy and polarization degrees of freedom, as well as other hybrid quantum states. To prove this, only the detection scheme should be adapted.

Combined with the simplicity of the design and its compact footprint, these results make the source an ideal device for future field experiments on quantum entanglement tests and quantum communication

networks. Particularly, the use of standard telecom components is well suited for integration in compact CubeSat platforms for satellite-based quantum networks. The overall approach can also be extended to free-space optics or a hybrid implementation with fiber components for extremely loss-sensitive experiments like loop-hole free tests of nonlocality or device-independent protocols. The versatile spectrally broadband source could be used for multi-user operation with variable temporal and spectral bandwidth allocation or high-capacity backbone channels with frequency division multiplexing, making it an ideal candidate for integration into flexible quantum network architectures of the future.

## 6. Methods

**Pump preparation.** A CW telecom laser operating at a center wavelength of 1560 nm is used as an initial pump source. If optical pulses are required for a certain application, they are carved from the laser by an intensity modulator (IM), controlled by an arbitrary waveform generator (AWG Tektronik 70002B), and amplified by an erbium-doped fiber amplifier (EDFA). The IM bias control and the total optical power are monitored by tapping a fraction of the optical power via fiber beam splitters. A tunable optical bandpass filter (BPF) placed thereafter spectrally purifies the pulses by removing the out-of-band amplified spontaneous emission originating from the amplifier. It is worth noting that the BPF (0.2 nm bandwidth) placed after the EDFA is narrower than the notch filter after the Sagnac loop to minimize any pump noise coupled to the detection system.

**Detection system.** A polarization-independent programmable filter (Finisar WaveShaper 16000A) is used to separate the signal and idler photons for the convenience of wavelength tunability. For both coarse and narrow demultiplexing filters, the isolation is  $\geq 35$  dB. To analyze the polarization entanglement of the photon pairs, we use a free-space polarization analysis module (PAM) for each photon of the pair, consisting of a half-wave plate (HWP) and a free-space PBS, from which we only detect one output. This setting allows us to have a constant polarization at the output of the PAM, which is more suitable for efficient detection with our superconducting nanowire single-photon detectors (SNSPD). The SNSPDs (SingleQuantum) are optimized for C-band operation and have specified detection efficiencies of  $\eta \approx 74\%$ , timing jitter of  $\sim 20$  ps and dead time of  $\sim 1$   $\mu$ s. Lastly, a time-to-digital converter (TDC; Qtools QuTAG with 1 ps resolution and 4.2 ps RMS time jitter) analyzes the photon-pair coincidences. We use a 120 ps coincidence window for coincidence event detection and 1 s of integration time.

**Loss characterization.** From the photon pair sources to the detection system, an average total loss of 12.85 dB are estimated, which breaks down as follows: 1 dB for the CIRC, 1.3 dB for the notch filter, 6 dB for the programmable optical filter, 3.25 dB insertion loss for the PAM and 1.3 dB detection loss. However, small asymmetries on each path lead to an overall detection efficiency for the signal channel  $\eta_s = -11.8$  dB, whereas for the idler channel it is  $\eta_i = -13.9$  dB. These significant losses can be reduced by at least 10 dB with low-loss components, particularly the DEMUX and PAM parts, but are tolerable to demonstrate the source functionality. We note that DEMUX of 1–2 dB loss are commercially available. Further, for reference, the fiber coupling loss of the SHG modules amounts to 0.5 dB for the 1550 nm fiber and 1–1.5 dB for the 780 nm fiber.

**Active state control.** The phase modulator has  $V_\pi = 4$  V at 50 kHz–2 GHz (iXblue). The peak voltages used for our phase modulator are  $\{0, +V_\pi, -V_{\pi/2}, +V_{\pi/2}\} = \{0, 250, -112.5, 112.5\}$  mV. The pulses are then amplified with an RF amplifier with  $\sim 28$  dB of fixed gain. To analyse the polarization of the entangled state, we include now in our previous PAM a quarter wave plate before the HWP to access the phase information.

## Funding

This work was financially supported by the Federal Ministry of Education and Research of Germany (BMBF) through the QuNET initiative.

## Acknowledgments


The presented results were partially acquired using facilities and devices funded by the Free State of Thuringia within the application center Quantum Engineering. MCP and CS are part of the Max Planck School of Photonics supported by BMBF, Max Planck Society, and Fraunhofer Society.

## Data availability statement

All data that support the findings of this study are included within the article (and any supplementary files).

## ORCID iDs

Meritxell Cabrejo-Ponce  <https://orcid.org/0000-0003-0451-3834>

Christopher Spiess  <https://orcid.org/0000-0002-5974-9177>

Fabian Steinlechner  <https://orcid.org/0000-0003-0122-1182>

## References

- [1] Steane A 1998 Quantum computing *Rep. Prog. Phys.* **61** 117–73
- [2] Slussarenko S and Pryde G J 2019 Photonic quantum information processing: a concise review *Appl. Phys. Rev.* **6** 041303
- [3] Xu F, Ma X, Zhang Q, Lo H-K and Pan J-W 2020 Secure quantum key distribution with realistic devices *Rev. Mod. Phys.* **92** 025002
- [4] Neumann S P, Selimovic M, Bohmann M and Ursin R 2022 Experimental entanglement generation for quantum key distribution beyond 1 Gbit/s (arXiv:2107.07756 [quant-ph])
- [5] Wengerowsky S, Joshi S K, Steinlechner F, Hübel H and Ursin R 2018 An entanglement-based wavelength-multiplexed quantum communication network *Nature* **564** 225–8
- [6] Joshi S K *et al* 2020 A trusted node-free eight-user metropolitan quantum communication network *Sci Adv.* **6** eaba0959
- [7] Kaltenbaek R, Blauensteiner B, Żukowski M, Aspelmeyer M and Zeilinger A 2006 Experimental interference of independent photons *Phys. Rev. Lett.* **96** 240502
- [8] Tsujimoto Y *et al* 2018 High-fidelity entanglement swapping and generation of three-qubit GHZ state using asynchronous telecom photon pair sources *Sci. Rep.* **8** 1446
- [9] Williams B P, Lukens J M, Peters N A, Qi B and Grice W P 2019 Quantum secret sharing with polarization-entangled photon pairs *Phys. Rev. A* **99** 062311
- [10] Grice W P, Beck M, Earl D, Mulkey D and Schaake J 2019 Reconfigurable entangled photon source (conference presentation) *Quantum Technologies and Quantum Information Science V* ed M T Gruneisen, M Dusek, J G Rarity and P M Alsing (Bellingham, WA: SPIE Optical Engineering Press) p 15
- [11] Anwar A, Perumangatt C, Steinlechner F, Jennewein T and Ling A 2021 Entangled photon-pair sources based on three-wave mixing in bulk crystals *Rev. Sci. Instrum.* **92** 041101
- [12] Li Y, Zhou Z-Y, Ding D-S and Shi B-S 2015 CW-pumped telecom band polarization entangled photon pair generation in a Sagnac interferometer *Opt. Express* **23** 28792
- [13] Vergyris P, Kaiser F, Gouzien E, Sauder G, Lunghi T and Tanzilli S 2017 Fully guided-wave photon pair source for quantum applications *Quantum Sci. Technol.* **2** 024007
- [14] Kim H, Kwon O and Moon H S 2019 Pulsed Sagnac source of polarization-entangled photon pairs in telecommunication band *Sci. Rep.* **9** 5031
- [15] Suo J, Dong S, Zhang W, Huang Y and Peng J 2015 Generation of hyper-entanglement on polarization and energy-time based on a silicon micro-ring cavity *Opt. Express* **23** 3985
- [16] Zhang M *et al* 2019 Generation of multiphoton quantum states on silicon *Light Sci. Appl.* **8** 41
- [17] Takesue H, Fukuda H, Tsuchizawa T, Watanabe T, Yamada K, Tokura Y and Itabashi S-i 2008 Generation of polarization entangled photon pairs using silicon wire waveguide *Opt. Express* **16** 5721–7
- [18] Zhou Q, Zhang W, Niu T-z, Dong S, Huang Y-d and Peng J-d 2013 A polarization maintaining scheme for 1.5  $\mu\text{m}$  polarization entangled photon pair generation in optical fibers *Eur. Phys. J. D* **67** 202
- [19] Chou M H, Brener I, Fejer M M, Chaban E E and Christman S B 1999 1.5  $\mu\text{m}$ -band wavelength conversion based on cascaded second-order nonlinearity in LiNbO<sub>3</sub> waveguides *IEEE Photon. Technol. Lett.* **11** 653–5
- [20] Jiang Y-K and Tomita A 2007 The generation of polarization-entangled photon pairs using periodically poled lithium niobate waveguides in a fibre loop *J. Phys. B: At. Mol. Opt. Phys.* **40** 437–43
- [21] Arahira S, Namekata N, Kishimoto T, Yaegashi H and Inoue S 2011 Generation of polarization entangled photon pairs at telecommunication wavelength using cascaded  $\chi^{(2)}$  processes in a periodically poled LiNbO<sub>3</sub> ridge waveguide *Opt. Express* **19** 16032
- [22] Zhang Z *et al* 2021 High-performance quantum entanglement generation via cascaded second-order nonlinear processes *npj Quantum Inf.* **7** 123–9
- [23] Agnesi C, Avesani M, Stanco A, Villoresi P and Vallone G 2019 All-fiber self-compensating polarization encoder for quantum key distribution *Opt. Lett.* **44** 2398
- [24] Li Y-P *et al* 2019 Experimental realization of a reference-frame-independent decoy BB84 quantum key distribution based on Sagnac interferometer *Opt. Lett.* **44** 4523
- [25] Li Y *et al* 2019 High-speed robust polarization modulation for quantum key distribution *Opt. Lett.* **44** 5262
- [26] Tanzilli S, Martin A, Kaiser F, De Micheli M P, Alibart O and Ostrowsky D B 2012 On the genesis and evolution of Integrated Quantum Optics: integrated quantum optics *Laser Photonics Rev.* **6** 115–43
- [27] Alibart O, D'Auria V, Micheli M D, Doutre F, Kaiser F, Labonté L, Lunghi T, Picholle É and Tanzilli S 2016 Quantum photonics at telecom wavelengths based on lithium niobate waveguides *J. Opt.* **18** 104001
- [28] Yao N *et al* 2020 Optimizing up-conversion single-photon detectors for quantum key distribution *Opt. Express* **28** 25123–33
- [29] Appas F, Baboux F, Amanti M I, Lemaitre A, Boitier F, Diamanti E and Ducci S 2021 Flexible entanglement-distribution network with an AlGaAs chip for secure communications *npj Quantum Inf.* **7** 118
- [30] Zhang W, Huang J, Zhang C, You L, Lv C, Zhang L, Li H, Wang Z and Xie X 2019 A 16-pixel interleaved superconducting nanowire single-photon detector array with a maximum count rate exceeding 1.5 GHz *IEEE Trans. Appl. Supercond.* **29** 1–4
- [31] Ma X, Fung C-H F and Lo H-K 2007 Quantum key distribution with entangled photon sources *Phys. Rev. A* **76** 012307
- [32] James D F V, Kwiat P G, Munro W J and White A G 2001 Measurement of qubits *Phys. Rev. A* **64** 052312
- [33] Turro S (Kwiat Quantum Information Group) 2021 *Guide to quantum state tomography* <http://research.physics.illinois.edu/QI/Photonics/tomography/>